

Ultrasonic Propagation in RbMnF_3 . III. F^{19} Nuclear Acoustic Resonance*

R. L. MELCHER† AND D. I. BOLEF

Arthur Holly Compton Laboratory of Physics, Washington University, St. Louis, Missouri 63130

(Received 4 March 1969)

The resonant coupling of coherent radio-frequency phonons to the F^{19} nuclear-spin system in antiferromagnetically ordered RbMnF_3 has been studied using a continuous-wave transmission spectrometer. With this technique, the resonant increase in the ultrasonic attenuation and/or the resonant dispersion in the phase velocity due to coupling with the spin system is detected. A phenomenological model of the spin-phonon interaction is developed which quite adequately explains the observed dependence of the nuclear-acoustic-resonance (NAR) signal strength on the orientation of the externally applied magnetic field. The two phenomenological nuclear-spin-phonon coupling constants g_1 and g_2 have the experimentally determined ratio $g_1/g_2 = 18.5 \pm 3.0$. The similarity of this ratio to the ratio of the magneto-elastic coupling constants $b_1/b_2 \gtrsim 10$ in this material is evidence that the observed spin-phonon interaction results from a magneto-elastically created virtual magnon which couples through the transferred hyperfine interaction to the F^{19} spin system to produce a spin transition. The temperature dependence of the signal strength is in good agreement with that predicted on the basis of the above coupling mechanism. The observed NAR line shape is quite complex and is found to depend on the temperature, power, and orientation.

I. INTRODUCTION

THE stimulation of nuclear-spin transitions by resonant externally generated radio-frequency phonons has been a useful technique for the study of nuclear-spin-phonon interactions for over a decade. Proctor and co-workers^{1,2} were the first to observe the saturation of the nuclear magnetization I_z due to ultrasonically induced spin transitions. Menes and Bolef³ showed that the resonant increase in ultrasonic attenuation due to the absorption of energy by the nuclear-spin system could be detected.

Until recently the only nuclear-spin-phonon interaction to be studied by this technique was the dynamic quadrupolar interaction,⁴ and thus the technique has been limited to the study of nuclei which possess a quadrupole moment. In the past few years, interest has developed in the possibility that strain-dependent internal magnetic interactions in magnetically ordered media could similarly produce a detectable nuclear-spin-acoustic-phonon interaction. This type of interaction is not restricted to spin- $I > \frac{1}{2}$ nuclei since it requires only that the nucleus possess a magnetic dipole moment.

Two types of internal dynamic magnetic interactions have been proposed theoretically. The first, due to Silverstein,⁵ is a two-step process involving an inter-

mediary virtual magnon state which is coupled through the static hyperfine interaction to the nuclear spins. The second interaction—the direct modulation by the elastic strain of the transferred hyperfine interaction between the magnetic moment of a magnetic ion and the nuclear spin of a neighboring nonmagnetic ion—has been treated by Buishvili and Giorgadze⁶ and more recently by Mahler and James.⁷

The rather scanty experimental facts thus far available show that some sort of internal magnetic nuclear-spin-phonon interaction exists in certain antiferromagnetically ordered materials. These experiments involve the F^{19} nuclear acoustic resonance (NAR) in KMnF_3 ⁸ and RbMnF_3 ^{9,10} and probably the Mn^{55} NAR in MnTe .¹¹ These investigations have not, however, yielded conclusive evidence as to the microscopic form of the nuclear-spin-phonon interaction.

In this paper an experimental study of the F^{19} NAR in antiferromagnetic RbMnF_3 is presented. The results lead to the conclusion that the Silverstein mechanism is responsible for the nuclear-spin-phonon interaction observed in this material. A brief outline of each of the two proposed coupling mechanisms is presented in Sec. II. Because of the difficulties encountered in applying the results of the present work directly to these theoretical models, a phenomenological model is also developed in Sec. II. In Sec. III a brief description of the experimental techniques used is given. The experimental results are presented in Sec. IV. Section V is devoted to a discussion of how the present results can be used to determine the microscopic origin of the spin-phonon

* Based in part upon a dissertation submitted by R. L. Melcher in partial fulfillment of the requirements for the Ph.D. degree at Washington University, St. Louis, Mo. Research sponsored in part by the National Science Foundation, under Grant No. GP 6881, and the U. S. Air Force Office of Scientific Research, under Grant No. 68-1412.

† National Science Foundation Graduate Fellow during most of the course of this research. Present address: Laboratory of Atomic and Solid State Physics, Cornell University, Ithaca, N. Y.

¹ W. G. Proctor and W. H. Tantilla, *Phys. Rev.* **101**, 1757 (1956).

² W. G. Proctor and W. A. Robinson, *Phys. Rev.* **104**, 1344 (1956).

³ M. Menes and D. I. Bolef, *Phys. Rev.* **109**, 218 (1958).

⁴ D. I. Bolef, in *Physical Acoustics*, edited by W. P. Mason (Academic Press Inc., New York, 1966), Vol. 4A.

⁵ S. D. Silverstein, *Phys. Rev.* **132**, 997 (1963).

⁶ L. L. Buishvili and N. P. Giorgadze, *Fiz. Tverd. Tela* **7**, 769 (1965) [English transl.: *Soviet Phys.—Solid State* **7**, 614 (1965)].

⁷ R. J. Mahler and L. W. James (private communication).

⁸ A. B. Denison, L. W. James, J. D. Currin, W. H. Tantilla, and R. J. Mahler, *Phys. Rev. Letters* **12**, 244 (1964).

⁹ R. L. Melcher, D. I. Bolef, and R. W. H. Stevenson, *Phys. Rev. Letters* **20**, 453 (1968).

¹⁰ R. L. Melcher and D. I. Bolef, *Phys. Rev. Letters* **20**, 1338 (1968).

¹¹ K. Walther, *Solid State Commun.* **5**, 399 (1967).

interaction. The results of our previous investigations of the elastic and magneto-elastic properties of RbMnF₃ (to be referred to as I¹² and II,¹³ respectively) will be used freely throughout this paper.

II. NUCLEAR-SPIN-PHONON COUPLING IN ANTIFERROMAGNETIC INSULATORS

A. Review of Microscopic Theories

1. Magnon coupled nuclear spin-phonon interaction

The strain dependence of the magnetocrystalline and dipolar anisotropy (i.e., the magneto-elastic coupling) provides a mechanism for coupling the magnetic and elastic modes of an antiferromagnetic crystal.¹³ In addition, the magnetic modes (magnons) are coupled to the nuclear-spin system through either the direct or the transferred hyperfine interaction. By taking a suitable average over the intermediate magnon states an effective nuclear-spin-phonon interaction can be obtained,⁵ which is linear in the nuclear-spin and elastic-strain operators. The stimulation of a nuclear-spin flip and the destruction of a phonon state can thus be described as a two-step process. The acoustic phonon creates a virtual magnon through the magneto-elastic interaction; the magnon is then coupled to the nuclear-spin system and produces a nuclear-spin flip via the static hyperfine interaction. The following expression is obtained for the NAR attenuation coefficient⁵:

$$\Delta\alpha_\lambda(\theta) = R \left(\frac{GA}{\omega_A} \right)^2 \frac{\omega^2 g(\omega)}{kT} \Gamma_\lambda(\theta), \quad (1)$$

where R is a temperature-independent constant. $\Gamma_\lambda(\theta)$ is an angular-dependent factor which for longitudinal and transverse acoustic waves, respectively, is given by

$$\begin{aligned} \Gamma_{\text{long}} &= \frac{1}{2} \sin^2 2\theta, \\ \Gamma_{\text{trans}} &= \frac{1}{2} \cos^2 2\theta. \end{aligned} \quad (2)$$

θ is the angle between the acoustic propagation direction and the direction of magnetic sublattice alignment. G is the single ion magneto-elastic coupling constant, A is the hyperfine constant, ω_A is the anisotropy frequency, and $g(\omega)$ is the line-shape factor at frequency ω . kT is the spin temperature in energy units.

2. Dynamic hyperfine interaction

The mechanism for the direct modulation of the magnetic interaction between the nuclear and ionic spins^{6,7} is somewhat more readily visualized. It depends simply on the strain dependence of the hyperfine interaction and as such is valid only for nuclei of non- or partially magnetic ions. This type interaction⁶ yields the same form of attenuation coefficient as does the

Silverstein mechanism [Eq. (1)], with the coupling constant GA/ω_A replaced by

$$GA/\omega_A \rightarrow \Lambda, \quad (3)$$

where Λ is the derivative of the hyperfine constant A with respect to the appropriate elastic strain.

The above calculations for $\Delta\alpha_\lambda(\theta)$ were made for uniaxial magnetic systems in magnetic fields which were low compared to the spin-flop field and at temperatures low enough that the noninteracting spin-wave approximation is valid. None of these conditions is satisfied in the present experiment, which makes a direct comparison of theory and experiment difficult. An alternative approach—the development of a phenomenological model valid at all temperatures $T \leq T_N$ —is considered in Sec. II B.¹⁴

B. Phenomenological Theory of NAR in RbMnF₃

The free-energy density of the coupled nuclear-spin and elastic systems may be written

$$E = E_N + E_E + E_{NE}. \quad (4)$$

The nuclear magnetic E_N and elastic E_E energy terms have the forms

$$E_N = -\mathbf{I} \cdot \mathbf{H}_0 \quad (5)$$

and

$$E_E = \frac{1}{2} C_{11} \sum_{i=x,y,z} e_{ii}^2 + \frac{1}{2} C_{44} (e_{xy}^2 + \text{c.p.}) + C_{12} (e_{xx}e_{yy} + \text{c.p.}), \quad (6)$$

where the C_{ij} are the adiabatic elastic constants, \mathbf{I} is the nuclear magnetization, c.p. denotes cyclic permutation, and the strains e_{ij} are defined in terms of the elastic displacements $u_i(\mathbf{r}, t)$ ($i = x, y, z$):

$$e_{ij} = \left(1 - \frac{1}{2} \delta_{ij} \right) \left(\frac{\partial u_i}{\partial x_j} + \frac{\partial u_j}{\partial x_i} \right). \quad (7)$$

The effective dc magnetic field \mathbf{H}_0 is related to the applied dc field \mathbf{H}_0' by

$$\mathbf{H}_0 = \mathbf{H}_0' (1 + \delta), \quad (8)$$

where

$$\delta = A_z \chi_m(T) / N g \beta \gamma_N \hbar \quad (9)$$

represents a fractional shift in the F¹⁹ nuclear resonance field because of the static transferred hyperfine interaction with the neighboring Mn²⁺ ions.¹⁵ χ_m is the molar electronic susceptibility, N is the Mn²⁺ number density, A_z is the hyperfine interaction component along \mathbf{H}_0 , g is, in general, dependent upon the orientation of \mathbf{H}_0 , g is the electronic g factor, β is the Bohr magneton, γ_N is the nuclear gyromagnetic ratio, and \hbar is Planck's constant

¹⁴ R. L. Melcher, Ph.D. thesis, Washington University, St. Louis, Mo., 1968 (unpublished).

¹⁵ M. B. Walker and R. W. H. Stevenson, Proc. Phys. Soc. (London) **87**, 35 (1966).

¹² R. L. Melcher and D. I. Bolef, Phys. Rev. **178**, 864 (1969).

¹³ R. L. Melcher and D. I. Bolef, Phys. Rev. **184**, 556 (1969).

divided by 2π . In the antiferromagnetic state of RbMnF_3 , $\delta \approx 0.03$.¹⁴

The form of the phenomenological nuclear-spin-phonon interaction E_{NE} may be deduced in the following manner. The F^{19} nucleus has spin $I = \frac{1}{2}$ and hence possesses no electric multipole moments; induced spin transitions must therefore be magnetic dipole transitions. Modulation of either direct or indirect nuclear magnetic dipole-dipole interactions has to be excluded on the basis of order-of-magnitude estimates of the coupling strength¹⁶ and the observation that no coupling can be detected for $T > T_N$.⁹ Thus, it can be concluded that E_{NE} is linear in the nuclear magnetization variables. To lowest order E_{NE} is also linear in the elastic strains and, in order to satisfy time-reversal symmetry, it is *postulated* to be linear in the electronic sublattice magnetization components. Under conditions of cubic symmetry one arrives at

$$E_{NE} = g_1 \sum_{i=x,y,z} M_i I_i e_{ii} + \frac{1}{2} g_2 [(M_x I_y + M_y I_x) e_{xy} + \text{c.p.}] \quad (10)$$

The g_1 and g_2 are phenomenological coupling constants, the M_i are the components of one of the sublattice magnetization vectors, and the I_i are the macroscopic nuclear magnetization components. There is no *a priori* justification for choosing the M_i to be the sublattice magnetization components rather than the components of the total magnetization. However, it should be noted that the total magnetization in fixed dc field \mathbf{H}_0 changes only very slightly in going from the paramagnetic to the antiferromagnetic state, whereas the spin-phonon coupling is found experimentally to be strongly dependent on the magnetic state of the system. In addition, it will be shown in Sec. IV that only the identification of the M_i with the sublattice magnetization results in good agreement with the observed dependence of the spin-phonon coupling on orientation of \mathbf{H}_0 . The results of the theory are of course independent of which sublattice is chosen.

To a good approximation the M_i in Eq. (10) are assumed to be constant quantities, independent of \mathbf{r} and t and of the small changes in \mathbf{H}_0 as the field is swept through the value for nuclear resonance. However, these sublattice magnetization components are strongly dependent on the orientation of \mathbf{H}_0 as described by the equilibrium orientation theory.¹⁷

The equations of motion of the nuclear magnetization variables and the elastic displacements are now solved under the assumption that the spin-phonon coupling produces only a small change in the phase velocity and in the attenuation of the elastic mode. This is the same approximation discussed in I and is always well satisfied in the present case. The equations of motion for the

nuclear magnetization in the reference frame ($\hat{X}, \hat{Y}, \hat{Z}$) in which the \hat{Z} axis is the axis of nuclear-spin quantization (for RbMnF_3 this corresponds to the direction of the applied magnetic field) are

$$\begin{aligned} \frac{dI_x}{dt} &= \gamma_N (\mathbf{I} \times \mathbf{H}^{(e)})_x - \frac{I_x}{\tau_N}, \\ \frac{dI_y}{dt} &= \gamma_N (\mathbf{I} \times \mathbf{H}^{(e)})_y - \frac{I_y}{\tau_N}, \\ \frac{dI_z}{dt} &\approx 0, \quad I_z \approx I_0 = \chi_0 H_0, \end{aligned} \quad (11)$$

where τ_N is the effective nuclear-spin-spin relaxation time, and where the linear approximation is assumed. χ_0 is the static nuclear susceptibility. The effective field acting on the nuclear magnetization is defined by

$$\mathbf{H}^{(e)} = -\frac{\partial E}{\partial \mathbf{I}}. \quad (12)$$

The equations of motion for the elastic displacements are given by

$$\rho \frac{\partial^2 u_x}{\partial t^2} = \frac{\partial^2 E}{\partial x \partial e_{xx}} + \frac{\partial^2 E}{\partial y \partial e_{xy}} + \frac{\partial^2 E}{\partial z \partial e_{xz}}, \quad (13)$$

with cyclic permutations of x , y , and z for u_y and u_z .

Solving the equations of motion in the linear approximation and assuming all quantities to vary harmonically in space and time, i.e., $\sim e^{i(\omega t - \mathbf{k} \cdot \mathbf{r})}$, the results for each mode can be written in terms of an effective elastic constant C_{ij}^* :

$$\rho v^2 \equiv C_{ij}^* = C_{ij} \frac{2g(g_1, g_2, M_i, \theta) \chi_0 \omega_0^2 \tau_N^2}{[1 + (\omega_0^2 - \omega^2) \tau_N^2 + 2i\omega \tau_N]}, \quad (14)$$

where C_{ij} is the "pure" elastic constant for that particular elastic mode, $v = \omega/k$ is the ultrasonic phase velocity, $g(g_1, g_2, M_i, \theta)$ is an angular-dependent coupling factor, $\omega_0 = \gamma_N H_0$, and θ is the angle between \mathbf{H}_0 and \mathbf{k} . Using $C_{ij} = \rho v_0^2$ and solving for the real and imaginary parts of v , one obtains

$$\Delta v = \text{Re}(v - v_0) = -\frac{g(g_1, g_2, M_i, \theta) \chi_0 \omega_0^2 \tau_N^2 v_0}{C_{ij}} \times \frac{1 + (\omega_0^2 - \omega^2) \tau_N^2}{[1 + (\omega_0^2 - \omega^2) \tau_N^2]^2 + 4\omega^2 \tau_N^2} \quad (15)$$

and

$$\Delta \alpha = k \text{Im}(v - v_0) = \frac{g(g_1, g_2, M_i, \theta) \chi_0 \omega_0^2 \tau_N^2}{C_{ij}} \times \frac{2\omega^2 \tau_N}{[1 + (\omega_0^2 - \omega^2) \tau_N^2]^2 + 4\omega^2 \tau_N^2}. \quad (16)$$

¹⁶ S. A. Al'tshuler, Zh. Eksperim. i Teor. Fiz. 24, 681 (1954); 28, 49 (1955) [English transl.: Soviet Phys.—JETP 1, 37 (1955)].

¹⁷ P. H. Cole and W. J. Ince, Phys. Rev. 150, 377 (1966).

TABLE I. Form of the nuclear-spin-acoustic-phonon interaction.

| Row | Elastic mode | Plane of H ₀ | C | $g(g_1, g_2, M_i, \theta)^a$ |
|-----|--|-------------------------|---|---|
| 1 | $\mathbf{k}_{\text{long}} \parallel [100]$ | (010) | C_{11} | $\frac{1}{2} g_1^2 M_x^2 \sin^2 \theta$ |
| 2 | $\mathbf{k}_{\text{long}} \parallel [100]$ | (0 $\bar{1}$ 1) | C_{11} | $\frac{1}{2} g_1^2 M_x^2 \sin^2 \theta$ |
| 3 | $\mathbf{k}_{\text{trans}} \parallel [100]$ $\mathcal{E} \parallel [001]$ | (010) | C_{44} | $\frac{1}{2} g_2^2 (M_x \cos \theta - M_y \sin \theta)^2$ |
| 4 | $\mathbf{k}_{\text{trans}} \parallel [100]$ $\mathcal{E} \parallel [010]$ | (010) | C_{44} | $\frac{1}{2} g_2^2 (M_x^2 + M_y^2 \sin^2 \theta)$ |
| 5 | $\mathbf{k}_{\text{long}} \parallel [110]$ | (1 $\bar{1}$ 0) | $\frac{1}{2} (C_{11} + C_{12} + 2C_{44})$ | $\frac{1}{16} [(g_1 - g_2)^2 (M_x - M_y)^2 + (g_1 + g_2)^2 (M_x + M_y)^2 \sin^2 \theta]$ |
| 6 | $\mathbf{k}_{\text{long}} \parallel [110]$ | (001) | $\frac{1}{2} (C_{11} + C_{12} + 2C_{44})$ | $\frac{1}{16} [(g_1 + g_2)^2 (M_x + M_y)^2 \sin^2 \theta + (g_1 - g_2)^2 (M_x - M_y)^2 \cos^2 \theta + 2(g_1 + g_2)(g_1 - g_2)(M_x^2 - M_y^2) \sin \theta \cos \theta]$ |
| 7 | $\mathbf{k}_{\text{trans}} \parallel [110]$ $\mathcal{E} \parallel [001]$ | (1 $\bar{1}$ 0) | C_{44} | $\frac{1}{16} g_2^2 [(M_x + M_y)^2 \cos^2 \theta + 2M_x^2 \sin^2 \theta - 2\sqrt{2} M_x (M_x + M_y) \sin \theta \cos \theta]$ |
| 8 | $\mathbf{k}_{\text{trans}} \parallel [110]$ $\mathcal{E} \parallel [001]$ | (001) | C_{44} | $\frac{1}{16} g_2^2 [(M_x + M_y)^2 + 2M_x^2 \sin^2 \theta]$ |
| 9 | $\mathbf{k}_{\text{trans}} \parallel [110]$ $\mathcal{E} \parallel [1\bar{1}0]$ | (1 $\bar{1}$ 0) | $\frac{1}{2} (C_{11} - C_{12})$ | $\frac{1}{16} g_1^2 [(M_x + M_y)^2 + (M_x - M_y)^2 \sin^2 \theta]$ |
| 10 | $\mathbf{k}_{\text{trans}} \parallel [110]$ $\mathcal{E} \parallel [1\bar{1}0]$ | (001) | $\frac{1}{2} (C_{11} - C_{12})$ | $\frac{1}{16} g_1^2 [(M_x - M_y) \sin \theta + (M_x + M_y) \cos \theta]^2$ |

^a θ is the angle between the direction of propagation of the elastic wave and the applied magnetic field.

$\Delta\nu$ is the dispersion and $\Delta\alpha$ the absorption of the elastic wave resulting from the coupling to the nuclear-spin system. Equation (16) may be put into a convenient form by defining a shape function $A(\tau_N, \chi_0, \omega)$ which is dependent only on the properties of the spin system and is independent of the type of elastic mode and the coupling parameters:

$$\Delta\alpha = \frac{g(g_1, g_2, M_i, \theta)}{C_{ij}} A(\tau_N, \chi_0, \omega). \quad (17)$$

The angular-dependent coupling factors $g(g_1, g_2, M_i, \theta)$ for the several possible elastic modes and orientations of \mathbf{H}_0 are summarized in Table I. Note that in addition to the explicit θ dependence of g , there is an implicit dependence as a result of the dependence of M_i on θ .

Using the fact that $\omega\tau_N \gg 1$, we may write the shape function $A(\chi_0, \omega, \tau_N)$

$$A(\chi_0, \omega, \tau_N) = \frac{\frac{1}{2} \chi_0 \omega^2 \tau_N}{1 + (\omega_0 - \omega)^2 \tau_N^2}, \quad (18)$$

which shows the Lorentzian shape expected of this type of analysis.

III. EXPERIMENTAL

The single-crystal specimens of RbMnF₃ and their preparation were described in I.¹²

Although the continuous-wave (cw) transmission spectrometer used in the present study has been de-

scribed elsewhere,¹⁸ a few of its most important features will now be discussed with emphasis on the reasons for its use in this study as a substitute for the more conventional marginal oscillator technique.⁴ Both methods are based on the measurement of small changes in the quality factor Q of the elastic standing-wave resonances produced in the specimen by a cw driving signal. A composite resonator (consisting of a single quartz transducer bonded to the specimen) is utilized in the tank circuit of the marginal oscillator; under the proper conditions the oscillator will lock onto the n th harmonic of vibration of the resonator. In the transmission spectrometer the composite resonator (consisting of two transducers bonded to opposite ends of the specimen) behaves similarly to a transmission-type cavity.

The transmission spectrometer has several advantages over the marginal oscillator in studying the F¹⁹ NAR in RbMnF₃. At the highest frequencies readily attained with the marginal oscillator (15–20 MHz) the magnetic-field-dependent elastic effects discussed in II are in most cases strong enough to obscure the NAR signal. By operating at 30 MHz with the transmission spectrometer we find these effects to be totally negligible. The strong dependence of the ultrasonic velocity (and therefore the standing-wave resonance frequency) on the temperature and magnetic field orientation in RbMnF₃ for $T < T_N$ requires frequent retuning of the impedance matching and inverting network when using

¹⁸ R. L. Melcher, D. I. Bolef, and J. B. Merry, Rev. Sci. Instr. 39, 1613 (1968).

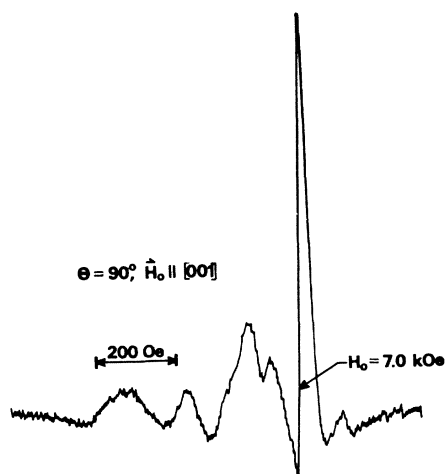


FIG. 1. Recorder trace of F^{19} NAR signal (first derivative) observed at $T=77.4$ K, for $k_{\text{ion}} \parallel [100]$, $H_0 \parallel [001]$, $\nu \approx 30$ MHz, with magnetic field modulation of 5 Oe peak-to-peak amplitude.

the marginal oscillator. In addition to being tedious, this introduces additional error into the relative signal strength measurements. The limited range of ultrasonic power densities available with the marginal oscillator makes saturation studies difficult; the transmission spectrometer is virtually unlimited in this respect.

Originally⁹ it was assumed that the very unusual NAR line shape observed in RbMnF_3 was due to the overlap of the F^{19} NAR spectrum with another absorption of unknown origin and that significantly higher frequencies would help unravel this set of absorption lines. As discussed in Sec. IV, this assumption was found to be wrong. However, the capability of going to the higher frequency was necessary in order to arrive at this conclusion.

It is readily shown¹⁸ that the signal obtained with the transmission spectrometer when using magnetic field modulation of peak-to-peak amplitude $(\Delta\omega_0/\gamma_N)$ is given by

$$S = \frac{2}{\alpha_0^2 + (\omega - \omega_{n0})^2} \left(-\alpha_0 \frac{\partial \Delta\alpha}{\partial \omega_0} + (\omega - \omega_{n0}) \frac{\partial \Delta\omega_n}{\partial \omega_0} \right) \Delta\omega_0, \quad (19)$$

where α_0 is the background attenuation, ω_{n0} is the standing-wave resonance frequency in absence of NAR dispersion, $\omega_0 = \gamma_N H_0$, ω is the rf carrier frequency, and $\Delta\alpha$ and $\Delta\omega_n$ are, respectively, the NAR absorption and the shift in the standing-wave resonance frequency due to NAR dispersion

$$\Delta\omega_n/\omega_{n0} = \Delta\nu/\nu_0. \quad (20)$$

All quantities in Eq. (19) are in units of rad/sec. By tuning the carrier frequency ω relative to ω_{n0} we can make the spectrometer sensitive to pure absorption or to a mixture of absorption and dispersion.¹⁰

The measurements reported in this paper were obtained using the transmission spectrometer at $\omega/2\pi \approx 30$

MHz, tuned for pure absorption ($\omega = \omega_{n0}$), and using magnetic field modulation. In all cases for which a comparison is possible, the present results agree with those reported earlier using the marginal oscillator technique at 12.2 MHz.⁹

IV. EXPERIMENTAL RESULTS AND COMPARISON TO PHENOMENOLOGICAL THEORY

A. F^{19} Nuclear Magnetic Resonance in RbMnF_3

A nuclear-magnetic-resonance (NMR) investigation of limited scope was undertaken using a conventional marginal oscillator spectrometer in order to ascertain which of the peculiarities of the NAR spectrum are properties of the F^{19} spin system itself and which are a result of the spin-phonon coupling mechanism. The results of the NMR study are summarized below.

1. *Dependence on orientation of applied field.* It has been well established¹⁵ that because of the anisotropic part of the hyperfine interaction [A_z in Eq. (9)], there exist, in general, three magnetically inequivalent F^{19} sites in the paramagnetic state of RbMnF_3 . Our NMR measurements at room temperature and at three frequencies (12, 16, and 24 MHz) confirm this behavior. In addition, measurements made at 77.4 and 55 K show that the same angular dependence exists in the antiferromagnetic state.

2. *Temperature dependence of δ .* According to Eq. (9), the fractional shift δ in the NMR field at fixed frequency is proportional to the static electronic susceptibility $\chi_m(T)$; the proportionality constant is to a good approximation independent of temperature. Measurements of $\delta(T)$ versus temperature¹⁴ from 4.2 to 300 K are in good agreement with the reported behavior of $\chi_m(T)$.¹⁹ For the high fields used in the NMR study (3–6 kOe), measurements of $\delta(T)$ yield a measure of the perpendicular susceptibility for $T < T_N$.²⁰ Since the F^- ion has two Mn^{++} nearest neighbors, one on each of the two oppositely oriented magnetic sublattices, even in the antiferromagnetic state the shift is proportional to the susceptibility χ_m rather than to the sublattice magnetization $M_i(T)$ as is the case in other less symmetric antiferromagnets.²¹

3. *Linewidth.* The width of the approximately Lorentzian F^{19} NMR line in the paramagnetic state is due to the magnetic interaction between the nuclear spin and the Mn^{++} ion as narrowed by the rapid exchange fluctuations of the Mn^{++} spin.²² Considering one component of the NMR spectrum (the less shifted of the two lines observed for $H_0 \parallel [100]$), one finds that the 17 ± 2 -Oe width (between first-derivative extrema) determined at $T=300$ K has narrowed to 13.5 ± 1 Oe at

¹⁹ W. J. Ince, M.S. thesis, MIT, 1965 (unpublished).

²⁰ S. Foner, in *Magnetism*, edited by G. T. Rado and H. Suhl (Academic Press Inc., New York, 1963), Vol. 1.

²¹ P. Heller, *Phys. Rev.* **146**, 403 (1966).

²² M. B. Walker, *Proc. Phys. Soc. (London)* **87**, 45 (1966).

$T \approx 90$ K. Below 90 K the width increases monotonically to a maximum of 35 ± 3 Oe at 4.2 K. No λ -type broadening is observed at $T \approx T_N$, in contrast to the results for the F^{19} NMR in MnF_2 ,²³ and KMnF_3 .²⁴ The symmetry of the F^{19} sites in RbMnF_3 is held to be responsible for the absence of any critical broadening effects.

B. NAR Line Shape, Linewidth, and Power Dependence

The unusual NAR line shape was originally believed to be due to the overlap of an additional absorption of unknown origin onto the F^{19} spectrum⁹; measurements made at 2.5 times the original frequency (and field), however, reveal qualitatively the same type of spectrum, indicating that the absorption is the result of the F^{19} spin system alone. Shown in Fig. 1 is the first-derivative signal obtained for $\mathbf{k}_{\text{long}} \parallel [100]$, $\mathbf{H}_0 \parallel [001]$, and $\nu \approx 30$ MHz. The line shape was found to be extremely sensitive to temperature, orientation of magnetic field, and to a limited extent to ultrasonic power density. Strong orientation dependence is expected due to the three inequivalent F^{19} sites. However, the line shape differs drastically from the approximately Lorentzian NMR lines observed at the same temperature and field orientation. In addition, its dependence on temperature and power lead to the conclusion that the unusual NAR line shape is in some way related to the nuclear-spin-phonon coupling mechanism.

Although the entire NAR spectrum (Fig. 1) is 500 Oe broad, the narrow, sharply peaked maximum (which coincides in field with the less shifted of the two NMR lines for this field orientation and frequency) has about the same width as the NMR line at this temperature (~ 20 Oe), and the variation of the width of this narrow maximum with temperature is identical to that of the NMR line to within the experimental accuracy. (This accuracy is limited by the temperature dependence of the line shape to $\sim \pm 20\%$.)

Spectra obtained for the same elastic mode and $\mathbf{H}_0 \parallel [101]$ and $\mathbf{H}_0 \parallel [100]$ are shown in Fig. 2. At

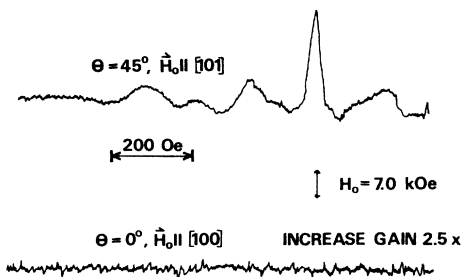


FIG. 2. Recorder trace of F^{19} NAR signal (first derivative) for the same temperature, elastic mode, and frequency as in Fig. 1. The magnetic field is aligned, respectively, along the $[101]$ and $[100]$ axes.

²³ P. Heller, Natl. Bur. Std. (U. S.) Misc. Publ. 273, 58 (1965).

²⁴ R. G. Shulman and K. Knox, Phys. Rev. 119, 94 (1960).

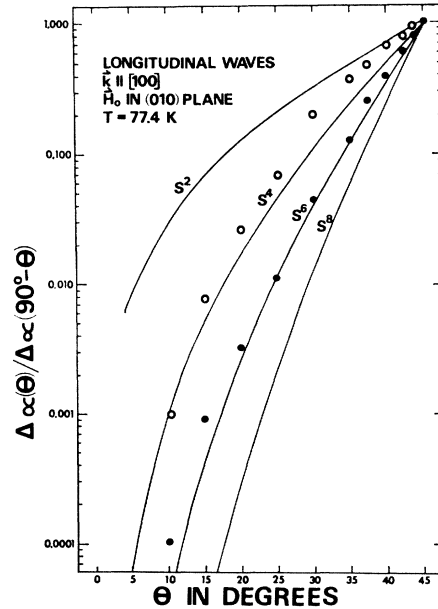


FIG. 3. Relative F^{19} NAR signal strength $\Delta\alpha(\theta)/\Delta\alpha(90^\circ-\theta)$ versus $\theta = \angle(\mathbf{H}_0, \mathbf{k})$; \mathbf{H}_0 in the (010) plane; $T = 77.4$ K, $\mathbf{k}_{\text{long}} \parallel [100]$; $\nu \approx 30$ MHz; $S^n = \sin^n \theta / \sin^n(90^\circ - \theta)$. Solid dots and open circles are, respectively, the data as corrected or not corrected for changes in the background attenuation.

lower temperatures ($50 \lesssim T \lesssim 60^\circ\text{K}$) the NAR spectra often more closely resemble the NMR spectra.¹⁰ The NAR signal strength at these lower temperatures is, however, much weaker.

C. Magnetic Field Orientation Dependence of the Spin-Phonon Interaction

In order to avoid errors introduced because of the orientation-dependent line shape, we make relative comparisons only between NAR spectra obtained for the magnetic field aligned along equivalent crystallographic directions. It is found experimentally that the line shape for fixed field orientation and temperature is essentially independent of the elastic mode. The discussion below refers exclusively to spectra obtained at $T = 77.4$ K.

The angular dependence of the spin-phonon coupling for $\mathbf{k}_{\text{long}} \parallel [100]$ and \mathbf{H}_0 in the (010) plane is presented in Fig. 3 [$\theta = \angle(\mathbf{H}_0, \mathbf{k})$]. By plotting $\Delta\alpha(\theta)/\Delta\alpha(90^\circ-\theta)$ versus θ one is assured of eliminating line-shape effects since the line shape is symmetric about $\theta = 45^\circ$. However, this type of plot can be somewhat misleading since any dependence of $\Delta\alpha(\theta)$ on θ which is symmetric about $\theta = 45^\circ$ is independent of θ when plotted as in Fig. 3. For comparison, the solid curves in Fig. 3 represent the functions $\sin^n \theta$, where $n = 2, 4, 6, 8$. The corrected data points are quite closely represented by a $\sin^6 \theta$ dependence. According to row 1 of Table I, the phenomenological theory predicts an angular dependence given by

TABLE II. Comparison of experimental results with phenomenological theory. (a) \mathbf{H}_0 applied along cubic axis; \mathbf{M} aligned along a face diagonal perpendicular to \mathbf{H}_0 . (b) \mathbf{H}_0 applied along face diagonal; \mathbf{M} aligned along body diagonal perpendicular to \mathbf{H}_0 .

| Row | Elastic mode | Orientation of \mathbf{H}_0 | Orientation of sublattice magnetization ^a | $(\Delta\alpha)_{\text{expt}}$ (sec ⁻¹) | Applicable row from Table I | $(\Delta\alpha)_{\text{theoret}}^b$ | Coupling constant ^c (10 ¹² erg/cm ³ sec) |
|-----|--|-------------------------------|--|---|-----------------------------|---|---|
| (a) | | | | | | | |
| 1 | $\mathbf{k}_{\text{long}} \parallel [100]$ | [001] | $M_x = M_y = M_0/\sqrt{2}$ $M_z = 0$ | 180 | 1 | $A_1 g_1^2 / 4C_{11}$ | $A_1 g_1^2 = 918$ |
| 2 | $\mathbf{k}_{\text{long}} \parallel [100]$ | [100] | $M_x = 0$ $M_y = M_z = M_0/\sqrt{2}$ | $\lesssim 0.02$ | 1 | 0 | ... |
| 3 | $\mathbf{k}_{\text{long}} \parallel [110]$ | [100] | $M_x = 0$ $M_y = M_z = M_0/\sqrt{2}$ | 37 | 6 | $\frac{1}{16} A_1 g_1^2$ $\frac{1}{2} (C_{11} + C_{12} + 2C_{44})$ | $A_1 g_1^2 = 705$ |
| 4 | $\mathbf{k}_{\text{trans}} \parallel [100]$ $\mathcal{E} \parallel [010]$ | [001] | $M_x = M_y = M_0/\sqrt{2}$ $M_z = 0$ | 0.77 | 4 | $\frac{1}{8} A_1 g_2^2 / C_{44}$ | $A_1 g_2^2 = 2.0$ |
| 5 | $\mathbf{k}_{\text{trans}} \parallel [100]$ $\mathcal{E} \parallel [010]$ | [100] | $M_x = 0$ $M_y = M_z = M_0/\sqrt{2}$ | $\lesssim 0.07$ | 4 | 0 | ... |
| 6 | $\mathbf{k}_{\text{trans}} \parallel [100]$ $\mathcal{E} \parallel [001]$ | [100] | $M_x = 0$ $M_y = M_z = M_0/\sqrt{2}$ | $\lesssim 0.02$ | 3 | 0 | ... |
| 7 | $\mathbf{k}_{\text{trans}} \parallel [100]$ $\mathcal{E} \parallel [001]$ | [001] | $M_x = M_y = M_0/\sqrt{2}$ $M_z = 0$ | $\lesssim 0.03$ | 3 | 0 | ... |
| (b) | | | | | | | |
| 8 | $\mathbf{k}_{\text{long}} \parallel [110]$ | [110] | $M_x = -M_y$ $= M_z = M_0/\sqrt{3}$ | 14 | 5, 6 | $\frac{1}{12} A_2 (g_1 - g_2)^2$ $\frac{1}{2} (C_{11} + C_{12} + 2C_{44})$ | $A_2 (g_1 - g_2)^2 = 197$ |
| 9 | $\mathbf{k}_{\text{long}} \parallel [110]$ | [1 $\bar{1}$ 0] | $M_x = M_y$ $= M_z = M_0/\sqrt{3}$ | 17 | 6 | $\frac{1}{12} A_2 (g_1 + g_2)^2$ $\frac{1}{2} (C_{11} + C_{12} + 2C_{44})$ | $A_2 (g_1 + g_2)^2 = 240$ |
| 10 | $\mathbf{k}_{\text{long}} \parallel [100]$ | [101] | $-M_x = +M_y$ $= M_z = M_0/\sqrt{3}$ | 20 | 1 | $\frac{1}{12} A_2 g_1^2 / C_{11}$ | $A_2 g_1^2 = 306$ |
| 11 | $\mathbf{k}_{\text{long}} \parallel [100]$ | [011] | $M_x = -M_y$ $= M_z = M_0/\sqrt{3}$ | 36 | 2 | $\frac{1}{6} A_2 g_1^2 / C_{11}$ | $A_2 g_1^2 = 276$ |
| 12 | $\mathbf{k}_{\text{trans}} \parallel [100]$ $\mathcal{E} \parallel [010]$ | [101] | $-M_x = M_y$ $= M_z = M_0/\sqrt{3}$ | 0.16 | 4 | $\frac{1}{16} A_2 g_2^2 / C_{44}$ | $A_2 g_2^2 = 0.84$ |
| 13 | $\mathbf{k}_{\text{trans}} \parallel [100]$ $\mathcal{E} \parallel [001]$ | [101] | $-M_x = M_y$ $= M_z = M_0/\sqrt{3}$ | 0.20 | 3 | $\frac{1}{12} A_2 g_2^2 / C_{44}$ | $A_2 g_2^2 = 0.79$ |

^a M_0 is the magnitude of the sublattice magnetization.

^b A_1 and A_2 characterize the line shape for $\mathbf{H}_0 \parallel$ (cubic axis) and $\mathbf{H}_0 \parallel$ (face diagonal), respectively.

^c Adiabatic elastic constants have been taken from I.

$M_x^2 \sin^2\theta$. For $\theta=0$, $M_x=0$, and for $\theta=90^\circ$, $M_x=\frac{1}{2}M_0$; thus, the predicted angular dependence is faster than $\sin^2\theta$, in agreement with the data of Fig. 3.

On the same type of plot the spin-phonon coupling for $\mathbf{k}_{\text{long}} \parallel [110]$, \mathbf{H}_0 in the (001) plane is given in Fig. 4. The angular dependence here is much weaker, showing a ratio of $\Delta\alpha(\theta)/\Delta\alpha(90^\circ) \simeq 0.81$. The good agreement of this behavior with the phenomenological theory is discussed below.

In order to obtain an experimental determination of the ratio of the two phenomenological coupling constants g_1 and g_2 , the experimental and theoretical results for several elastic modes and for two magnetic field orientations are summarized in Tables II(a) and II(b). A_1 and A_2 are the experimental shape functions observed, respectively, for $\mathbf{H}_0 \parallel$ (cubic axis) and $\mathbf{H}_0 \parallel$ (face

diagonal). In Table II(a) the field is aligned along a cubic axis of the specimen. From the equilibrium theory¹⁷ the sublattice magnetization is known to lie along one of the equivalent face diagonals in the plane perpendicular to \mathbf{H}_0 . One of the four possible orientations of a given sublattice magnetization is given in column 4 of Table II(a). Other allowed choices of orientation, when used in the coupling constants obtained from the phenomenological theory (Table I), yield results equivalent to those shown in column 7 of Table II(a) for the NAR attenuation coefficient $\Delta\alpha$. In the last column, obtained by using the experimental results (column 5), are listed the values of the shape function [Eq. (18)] times the square of the appropriate coupling constant. The shape function is constant for a given orientation of \mathbf{H}_0 and temperature.

The results for \mathbf{H}_0 parallel to a face diagonal are presented in Table II(b). For this orientation of \mathbf{H}_0 the sublattice magnetization vectors are aligned along a body diagonal in the plane perpendicular to \mathbf{H}_0 .¹⁷

In each of the 13 cases considered in Table II good agreement with the predictions of the phenomenological theory is found. All of these results are consistent with the following ratio of the two phenomenological coupling constants g_1 and g_2 :

$$g_1/g_2 = 18.5 \pm 3.0. \quad (21)$$

The consequences of these results in terms of the microscopic models are discussed in Sec. V.

D. Temperature Dependence of Spin-Phonon Interaction

Several factors inhibit the accurate measurement of the temperature dependence of the spin-phonon coupling. The temperature-dependent line shape makes it very difficult to estimate accurately the area under the absorption curve. The background ultrasonic attenuation in RbMnF_3 in the region of interest is a sharp function of temperature (a result of the magnetoelastic effects discussed in I and II) and must be corrected for through the use of Eq. (19). Care must be taken to adjust the ultrasonic power density in the specimen to a level low enough to avoid saturation at each temperature. The rapidly changing background attenuation makes the power density in the specimen quite sensitive to temperature. Finally, Eq. (19) is strictly valid only for Lorentzian standing-wave resonances—a condition which is only very crudely approximated for $T \lesssim 70$ K because of the strong magneto-elastic coupling for $50 \lesssim T \lesssim 70$ K.¹²

The experimental behavior shown in Fig. 5 is for longitudinal waves propagating along the $[110]$ axis with $\mathbf{H}_0 \parallel [010]$. Equation (19) has been used to correct for the temperature-dependent background attenuation, but no attempt has been made to correct for the temperature dependence of the line shape. The general temperature dependence is unmistakable; the signal strength reaches a maximum at $T \approx 73$ K and is unobservable for $T > T_N$ or $T \lesssim 50$ K. This same general behavior has been observed for other elastic modes and magnetic field orientations (e.g., see Ref. 9).

Even though Silverstein's calculation⁵ uses the non-interacting spin-wave approximation, he also demonstrates that for the case of $H_0 = 0$ the same result can be obtained using a semiclassical model. To within the accuracy of the molecular field model it is straightforward to extend this calculation and obtain an expression for the temperature dependence of the NAR attenuation coefficient, valid at all temperatures $T < T_N$:

$$\Delta\alpha_\lambda(T) \sim \left(\frac{b_\lambda(T)M_0(T)}{K(T)} \right)^2 \frac{1}{T}, \quad (22)$$

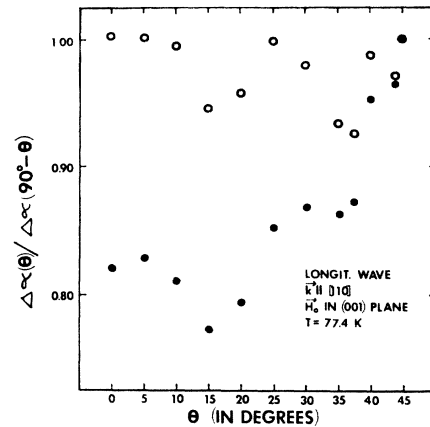


FIG. 4. Relative F^{19} NAR signal strength versus $\theta = \angle(\mathbf{H}_0, \mathbf{k})$; \mathbf{H}_0 in (001) plane; $T = 77.4$ K; $\mathbf{k}_{\text{long}} \parallel [110]$; $\nu \approx 30$ MHz. Solid dots and open circles are, respectively, the data as corrected and not corrected for changes in the background attenuation.

where the phenomenological magneto-elastic coupling constant $b_\lambda(T)$ includes contributions from the crystalline field [i.e., G of Eq. (1)] and the strain dependence of the dipolar interaction between Mn^{++} ions,²⁵ and $K(T) = (2\omega_A/\gamma_e)M_0$ is the anisotropy constant. Although Eq. (22) is strictly valid only for $H_0 = 0$, it is not expected that application of a magnetic field will cause significant changes in the temperature dependence. Using the experimental values of $b_\lambda(T)$ ²⁵ and $K(T)$ ²⁶ for RbMnF_3 and the Brillouin function for $M_0(T)$, Eq. (22) is plotted in Fig. 5 (solid line). The agreement with the experimental points is far better

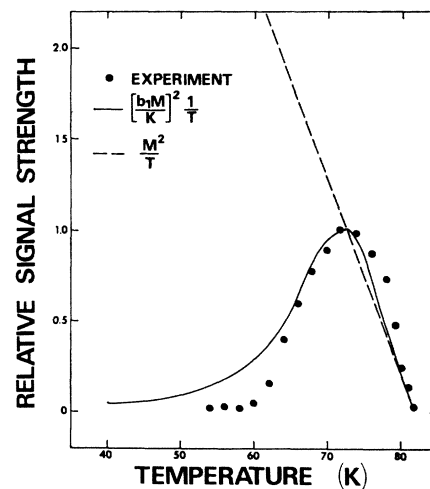


FIG. 5. Relative F^{19} NAR signal strength versus temperature; $\mathbf{k}_{\text{long}} \parallel [110]$; $\mathbf{H}_0 \parallel [010]$; $\nu \approx 30$ MHz; solid dots are the experimental data as corrected for background attenuation changes; solid line is the function $(b_1 M_0 / K)^2 1/T$ and the dashed line is the function M_0^2 / T . The data have been normalized to one at $T = 73$ K.

²⁵ D. E. Eastman, Phys. Rev. **156**, 645 (1967).

²⁶ M. J. Freiser, R. J. Joenk, P. E. Seiden, and D. T. Teaney, in *Proceedings of the International Conference on Magnetism, Nottingham, 1964* (The Institute of Physics and The Physical Society, London, 1965), p. 432.

than one should expect if the scatter in the $b_\lambda(T)$ and $K(T)$ data used in plotting Eq. (22) is taken into consideration.

At low temperatures ($T \lesssim 10$ K), Eq. (22) predicts an increase in $\Delta\alpha_\lambda(T)$ as the $1/T$ factor dominates. This is not observed experimentally, presumably because of saturation. At temperatures as high as 60 K difficulty in avoiding saturation was encountered.

In the same molecular field approximation the temperature dependence of the direct interaction⁶ involving the strain gradients of the hyperfine interaction is given by

$$\Delta\alpha_\lambda(T) \sim M_0^2(T)/T. \quad (23)$$

In both Eqs. (22) and (23) the hyperfine constant A and its strain derivatives Λ have been assumed to be temperature-independent. Equation (23) has also been plotted on Fig. 5 (dashed line). For $T \lesssim 73$ K the temperature dependence predicted by this coupling mechanism is quite different from that observed experimentally. In Fig. 5 the experimental data and the two theoretical curves [Eqs. (22) and (23)] have been normalized to one curve at $T = 73$ K.

V. DISCUSSION AND CONCLUSIONS

The phenomenological model presented in Sec. II B has been found in Sec. IV to give an excellent description of the dependence of the spin-phonon coupling strength on the orientation of the applied field. Each elastic mode and field orientation considered experimentally is consistent with this model and with a more-than-order-of-magnitude difference between the phenomenological coupling constants g_1 and g_2 .

The two independent magneto-elastic coupling constants of RbMnF_3 (b_1 and b_2) have been found experimentally to be in the ratio^{13,25} $b_1/b_2 \gtrsim 10$. Each elastic mode may be shown¹³ to be coupled to the magnetic modes by either b_1 or b_2 or $b_1 \pm b_2$ (Table I of II). Comparing Table I of II with Table II of the present

paper, one sees that those modes coupled to the magnetic system by b_1 are precisely those whose nuclear-spin-phonon interaction is determined by g_1 , and similarly for b_2 and g_2 and for $b_1 \pm b_2$ and $g_1 \pm g_2$. Although the angular dependences predicted by the two microscopic models^{5,6} are the same, the similarity of the experimental ratios g_1/g_2 and b_1/b_2 strongly suggests that magneto-elastic coupling plays an important role in the observed nuclear-spin-phonon coupling. Only in the two-step mechanism suggested by Silverstein⁵ does magneto-elastic coupling play a role.

The agreement of the observed temperature dependence with that predicted by a simple extension of the Silverstein theory is additional evidence that it is this mechanism which is responsible for the results observed in the present experiments on RbMnF_3 .

Serious questions concerning the spin-phonon interaction remain unresolved. These questions are centered around the unusual line shape and its dependence on temperature, ultrasonic power, and magnetic field orientation.

Note added in proof. Assuming that the magnon coupled nuclear spin-phonon interaction (see Sec. II A) is responsible for the observed resonant absorption, the anisotropy of the transferred hyperfine interaction¹⁵ leads to the result that magnetically inequivalent F^{19} nuclear spins will experience different spin-phonon coupling constants. Taking this anisotropy into account, one finds for the case considered in Fig. 1 that two absorption lines are expected, the ratio of whose intensities is 5.4:1. Although this does not explain the structure shown in Fig. 1, it demonstrates one way in which the observed NAR absorption spectrum is expected to differ from the NMR spectrum.

ACKNOWLEDGMENT

Dr. R. W. H. Stevenson kindly provided the single crystal samples of RbMnF_3 used in this work.